NANO LETTERS

pubs.acs.org/NanoLett

Letter

# Pressure-Tuned Intralayer Exchange in Superlattice-Like $MnBi_2Te_4/(Bi_2Te_3)_n$ Topological Insulators

Jifeng Shao,[‖] Yuntian Liu,[‖] Meng Zeng, Jingyuan Li, Xuefeng Wu, Xiao-Ming Ma, Feng Jin, Ruie Lu, Yichen Sun, Mingqiang Gu, Kedong Wang, Wenbin Wu, Liusuo Wu, Chang Liu, Qihang Liu,* and Yue Zhao*

Cite This: *Nano Lett.* 2021, 21, 5874−5880

Read Online

ACCESS | Metrics & More | Article Recommendations | Supporting Information

**ABSTRACT:** The magnetic structures of $MnBi_2Te_4(Bi_2Te_3)_n$ can be manipulated by tuning the interlayer coupling via the number of $Bi_2Te_3$ spacer layers $n$, while the intralayer ferromagnetic (FM) exchange coupling is considered too robust to control. By applying hydrostatic pressure up to 3.5 GPa, we discover opposite responses of magnetic properties for $n = 1$ and 2. $MnBi_4Te_7$ stays at A-type antiferromagnetic (AFM) phase with a decreasing Néel temperature and an increasing saturation field. In sharp contrast, $MnBi_6Te_{10}$ experiences a phase transition from A-type AFM to a quasi-two-dimensional FM state with a suppressed saturation field under pressure. First-principles calculations reveal the essential role of intralayer exchange coupling from lattice compression in determining these magnetic properties. Such magnetic phase transition is also observed in 20% Sb-doped $MnBi_6Te_{10}$ because of the in-plane lattice compression.

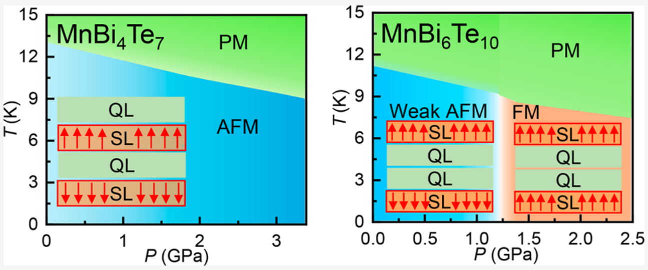


**KEYWORDS:** *magnetic topological insulator, hydrostatic pressure, quasi-two-dimensional ferromagnetic state, first-principles calculations, intralayer exchange coupling*

In magnetic topological insulators (MTI), the interplay between magnetic order in real space and the topological electronic structure in momentum space gives rise to many novel topological matters and emergent quantum phenomena, such as Weyl Fermions, quantum anomalous Hall effect (QAHE), axion insulator phase, and chiral Majorana modes.[1−6] A prototypical example is the layered intrinsic MTI $MnBi_2Te_4$ with the local moments of Mn atoms ferromagnetic (FM) aligned within one layer while adopting an A-type antiferromagnetic (AFM) order along the stacking direction.[7−12] By manipulating the magnetic order in few-layer $MnBi_2Te_4$ using film thickness and magnetic field, various topological phases have been experimentally realized, including zero-field QAHE and tunable axion insulator and other high-order Chern insulator phases.[13−19]

In the family of $MnBi_2Te_4(Bi_2Te_3)_n$, the interplay of magnetism and topology can be further enriched by inserting $n$ layers of nonmagnetic topological insulator (TI) $Bi_2Te_3$ into the van der Waals layered MTI $MnBi_2Te_4$.[20−32] Such heterostructure engineering of the nonmagnetic TI and MTI building blocks not only reveals termination-dependent surface states and hybridization between different building blocks[25] but also effectively tunes the interlayer exchange coupling (IEC) between the neighboring magnetic layers, leading to new topological phases associated with different magnetic phases.[27,30,31] For $n = 1$, the transport and magnetism study of $MnBi_4Te_7$ shows an A-type AFM state right below Néel temperature ($T_N$) and a competing magnetic order of FM state at an even lower temperature ($T \sim 1$ K).[22] As $n$ goes to 2, with a further weakened interlayer coupling between the magnetic layers, $MnBi_6Te_{10}$ keeps a relatively weak A-type AFM ground-state behavior, with enhanced hysteresis loops in the magnetization curves below 6 K.[29] Such magnetic behaviors could be associated with the competition between the weak interlayer exchange coupling and other magnetic interactions.[22,32] Despite the complicated magnetism, a quasi-two-dimensional (2D) ferromagnet is proposed to dominate the magnetic properties at large $n$ ($n \geqslant 3$) with a vanishing interlayer coupling.[30,31] On the other hand, the intralayer exchange coupling is typically considered as robust FM and thus difficult to manipulate by experimentally accessible "knobs".

As a clean, nonintrusive, reversible, and continuous structure tuning technique, hydrostatic pressure is usually utilized to

**Received:** May 13, 2021
**Revised:** June 27, 2021
**Published:** July 1, 2021

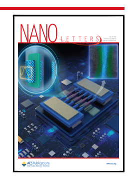







https://doi.org/10.1021/acs.nanolett.1c01874
*Nano Lett.* 2021, 21, 5874−5880

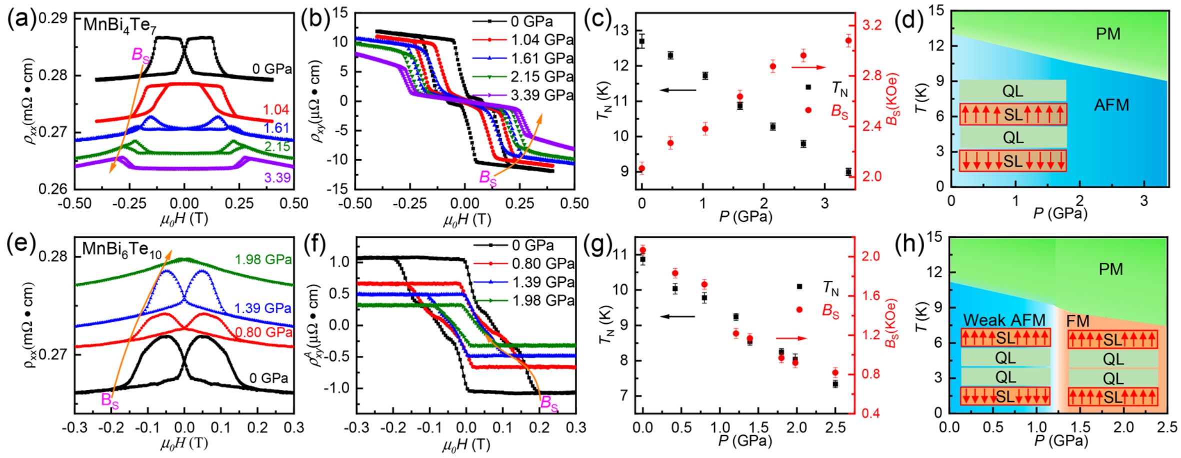


**Figure 1.** Pressure tuned magnetism of $MnBi_4Te_7$ and $MnBi_6Te_{10}$. (a,b) Field dependence of the magneto-resistivity $\rho_{xx}$ (a) and the Hall resistivity $\rho_{xy}$ (b) of $MnBi_4Te_7$ at $T = 2$ K under different pressure from 0 to 3.39 GPa. The curves of magneto-resistivity at zero pressure are shifted for clarity. (e,f) Field dependence of $\rho_{xx}$ and the anomalous Hall resistivity $\rho_{xy}^A$ of $MnBi_6Te_{10}$ at $T = 2$ K under different pressure. An FM phase occurs for $MnBi_6Te_{10}$ at 1.98 GPa. The orange curved arrows mark the change of saturation field as pressure increases. The evolution of magnetic phase transition temperature (black square) and saturation field (red dot) with pressure are summarized for $MnBi_4Te_7$ (c) and $MnBi_6Te_{10}$ (g). The magnetic ordering temperature decreases for both crystals as increasing pressure, while the saturation field responds differently. (d) and (h) are the schematic phase diagrams of $MnBi_4Te_7$ and $MnBi_6Te_{10}$, respectively. SL and QL represent the $MnBi_2Te_4$ septuple layer and the $Bi_2Te_3$ quintuple layer.

modify the interlayer coupling strength by adjusting the interlayer separation in van der Waals structures.[33−36] In this work, by applying hydrostatic pressure up to 3.5 GPa, we found in $MnBi_2Te_4(Bi_2Te_3)_n$ ($n$ = 1 and 2) distinct evolution of magnetic properties originated from the manipulation of intralayer exchange coupling. In contrast to the increasing saturation field in $MnBi_4Te_7$ ($n$ = 1), the saturation field of $MnBi_6Te_{10}$ ($n$ = 2) decreases by half to about 0.1 $T$ at high pressure. In particular, an FM-like hysteresis of anomalous Hall resistivity and magnetic susceptibility emerges at 1.98 GPa, where the kinks or plateaus associated with AFM state between the polarized FM states vanish completely, suggesting the formation of FM domains. Our first-principles calculation shows that although the interlayer exchange coupling increases with pressure for both $n$ = 1 and 2, hydrostatic pressure reduces the intralayer FM exchange coupling by evoking the competition between the AFM-preferred direct exchange and FM-preferred superexchange coupling within the $MnBi_2Te_4$ layer. Considering the nearly vanishing interlayer coupling in $MnBi_6Te_{10}$ (about 0.01 meV, one order less compared with $MnBi_4Te_7$), the weakening of the intralayer FM exchange coupling will enhance the effect of fluctuation, including magnetic domains, thermal fluctuation, and other magnetic perturbations. The reduced intralayer magnetization can in turn decrease the interlayer exchange coupling strength (IEC $\propto m_s$) in pressurized $MnBi_6Te_{10}$, and effectively decouple the adjacent magnetic layers, leading to a magnetic phase transition from weak A-type AFM to quasi-2D-FM state. A similar FM state is also observed in Sb-doped $MnBi_6Te_{10}$ with comparable in-plane lattice compression, providing additional evidence that reduced intralayer FM coupling can decouple the magnetic layers in weakly interlayer coupled MTI. Our results first reveal the delicate role of intralayer exchange coupling in the complex magnetic properties in MTI/TI heterostructures with a variable number of nonmagnetic layers.

The single crystals were grown by flux method and first characterized by single-crystal XRD on both the top and bottom surfaces (Figure S1). Subsequent screening using magnetic and magneto-transport measurements at ambient pressure was operated before applying high pressure (Figure S2 and S3). The measurement details under high pressure are described in the Supporting Information.

Figure 1a,b present the horizontal and Hall resistivity of $MnBi_4Te_7$ at various pressure at $T = 2$ K. As pressure increases gradually to 3.39 GPa, the saturation field $B_s$ increases from 2.07 to 3.08 kOe, and the hysteresis loops are strongly inhibited, indicating enhanced AFM interlayer exchange coupling. However, with increasing pressure, we observe a monotonic decrease of Néel temperature from 12.7 to 9 K, directly contrasting to what could be expected at an enhanced AFM interlayer exchange coupling.

Figure 1e,g show the pressure-tuned transport behavior of $MnBi_6Te_{10}$. At ambient pressure, the weakened kinks around zero moment in the hysteresis loop mark the reduced interlayer AFM exchange coupling in $MnBi_6Te_{10}$ as $n$ increases. Similar to $MnBi_4Te_7$, the magnetic phase transition temperature of $MnBi_6Te_{10}$ also decreases with increasing pressure. However, as pressure increases, the saturation field of $MnBi_6Te_{10}$ gradually decreases from 0.2 to 0.08 T (Figure 1g). The responses to pressure of both the saturation field and magnetic ordering temperature of $MnBi_6Te_{10}$ are reversible, as shown in Figure S4d. The changes are inconsistent with the expected enhanced AFM interlayer coupling with compression along the $c$-axis. Note that the magnetic ordering temperature of $MnBi_4Te_7$ (∼13 K),[22,24] $MnBi_6Te_{10}$ (∼11 K),[27−29] and $MnBi_8Te_{13}$ (∼10.5 K)[30,31] are close to that of monolayer $MnBi_2Te_4$ (∼12 K),[14] the decreased magnetic ordering temperature could be related to the lattice compression within the magnetic septuple layer, since hydrostatic pressure simultaneously compresses the in-plane and out-of-plane lattice parameters.

Moreover, a relatively pure FM state emerges at pressure above 1.39 GPa, evidenced by a butterfly-shaped magnetoresistance and disappeared kinks associated with the weak AFM states in anomalous Hall resistance curves. Since no structural phase transitions are expected under pressure below


https://doi.org/10.1021/acs.nanolett.1c01874
Nano Lett. 2021, 21, 5874−5880

6 GPa in $Bi_2Te_3$, $MnBi_2Te_4$, and $MnBi_4Te_7$ single crystals,[37−39] it is quite counterintuitive that an FM state emerges as the pressure-induced compression along *c*-axis will strengthen the AFM interlayer exchange coupling.

To confirm the magnetic phase transition in $MnBi_6Te_{10}$, we applied the magnetic susceptibility and magnetization measurements under high pressure using a precalibrated Hall sensor. Measurement details are described in the Supporting Information. Figure 2 shows the temperature dependence of the magnetic susceptibility and the magnetization curves of $MnBi_6Te_{10}$ under different pressure with $H$ // $c$. The $M-T$ curve at ambient pressure measured by our method shows bifurcation of the zero-field cooling (ZFC) and field cooling (FC) at $T_N$, which matches well with the $M-T$ curves directly measured by VSM, see Figure S8b. As pressure increases, the ZFC curve changes from a sharp cusp-like shape to a flat dome with increasing FC susceptibility below the magnetic phase transition temperature. The number of peaks on $dM/dH-H$ curve reduces to 2 at 1.98 GPa, marking the spin changes between up and down two states, see Figure 2b. Magnetization measurements show that the sample goes back to its original AFM behavior after releasing the pressure (Figure S5). Based on the experimental observations in both the magneto-transport and magnetization measurements, we conclude that an FM phase transition indeed occurs in $MnBi_6Te_{10}$ as pressure increases.

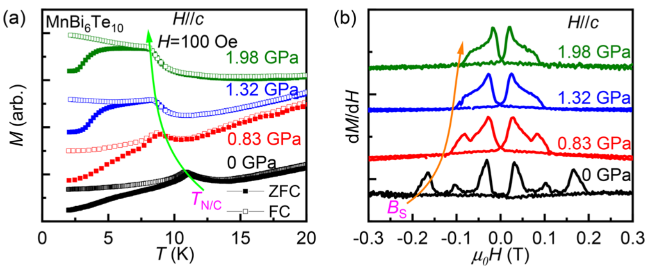


**Figure 2.** Magnetic susceptibility measurements of $MnBi_6Te_{10}$ under pressure. (a) Temperature dependence of zero-field-cooled (ZFC) and field-cooled (FC) magnetic susceptibility of $MnBi_6Te_{10}$ measured by Hall sensor method at different pressures under an applied magnetic field of 100 Oe along *c*-axis. (b) Isothermal magnetization of $MnBi_6Te_{10}$ at 2 K at various pressure with magnetic field along *c*-axis. The curves are shifted for clarity. The green and orange curved arrows mark the evolution of magnetic ordering temperature and saturation field with increasing pressure, respectively.

The magnetic ground states of the layered $MnBi_2Te_4(Bi_2Te_3)_n$ compounds are the results of both interlayer and intralayer exchange coupling. While the interlayer coupling is dictated by the superexchange between Mn-3d orbitals in adjacent layers mediated by the p orbitals of Bi and Te atoms in between, the intralayer coupling is determined by the competition between the superexchange and direct exchange, as shown in Figure 3a. The former is between two adjacent Mn atoms mediated by a Te atom with a calculated Mn−Te−Mn bond angle of about 95°. Thus, the superexchange coupling prefers FM state according to the Goodenough−Kanamori−Anderson (GKA) rule.[40,41] The latter prefers AFM coupling because the direct FM hopping between Mn atoms is forbidden for $Mn^{2+}$ high-spin state ($d^5$). Because of the large Mn−Mn distance (about 4.4 Å), the direct exchange coupling is much smaller than the superexchange. Therefore, the intralayer FM state is dominant in $MnBi_2Te_4(Bi_2Te_3)_n$.

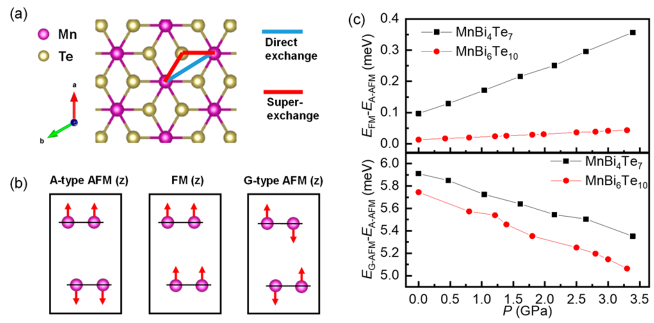


**Figure 3.** (a) Schematic of the stacking of Mn and its adjacent Te layers with top view, showing the intralayer exchange coupling within a magnetic layer of $MnBi_2Te_4$. The intralayer coupling is determined by the competition of the direct exchange coupling between two adjacent Mn atoms (blue) and the superexchange coupling mediated by Te atoms (red). (b) Schematics of the magnetic configurations for A-AFM, FM, and G-AFM phases. The red arrows represent the direction of the magnetic moments. (c) Top panel: the energy difference between FM and A-AFM phases for $MnBi_4Te_7$ and $MnBi_6Te_{10}$ at different pressure; bottom panel: the energy difference between G-AFM and A-AFM phases for $MnBi_4Te_7$ and $MnBi_6Te_{10}$ as pressure changes.

To understand the different magnetic behaviors of $MnBi_4Te_7$ and $MnBi_6Te_{10}$ under pressure, we employ the Heisenberg model to study the interlayer and intralayer exchange coupling parameters in these materials (details can be found in the Supporting Information). Our simulation uses three different magnetic configurations: G-type AFM, A-type AFM, and FM (Figure 3b) to evaluate the strength of the interlayer and intralayer couplings, which can be expressed by the total energy difference $E_{FM} - E_{A\text{-}AFM}$, and $E_{G\text{-}AFM} - E_{A\text{-}AFM}$, respectively. Our calculation shows that the hydrostatic pressure causes the lattice to shrink both along and perpendicular to the stacking direction (Figure S9). However, hydrostatic pressure monotonically increases the strength of interlayer exchange coupling but decreases the strength of intralayer coupling by about 10% (Figure 3c). The weakened intralayer coupling can be explained by the competition between direct exchange and superexchange. In our calculation, when the pressure increases to 3 GPa, both the Mn−Te bond length and the distance between Mn atoms decrease by about 2%, while the Mn−Te−Mn bond angles are almost unchanged. Thus, the AFM-preferred direct exchange, which has a higher power of correlation to the distance ($\sim d_{Mn-Mn}^{-5}$),[42,43] will increase much more than superexchange. Considering the decreasing intralayer FM coupling, the effects of fluctuations, including magnetic domains, thermal fluctuations, and other magnetic perturbations, become more pronounced as pressure increases. The combined effect will reduce intralayer magnetization, causing a decreased magnetic transition temperature and anomalous Hall resistivity for both $MnBi_4Te_7$ and $MnBi_6Te_{10}$ in Figure 1.

The distinct behavior of $B_s$ and magnetic ground state for different $MnBi_2Te_4(Bi_2Te_3)_n$ under pressure can thus be understood by investigating the change of interlayer and intralayer exchange coupling for different numbers of $Bi_2Te_3$ spacing layers $n$. The intralayer magnetization decreases similarly for $MnBi_4Te_7$ ($n$ = 1) and $MnBi_6Te_{10}$ ($n$ = 2), as DFT calculation shows weakened intralayer FM coupling with increasing pressure (Figure 3c). The decreased total magnetic moment ($m_s$) from one magnetic septuple layer leads to a negative contribution to the interlayer exchange coupling (IEC $\propto m_s$).[33,44] Such a reduced intralayer magnetization effect will not be captured by the DFT calculated change of interlayer coupling because DFT calculation considers a perfect unit cell with certain magnetic configurations at zero temperature. Considering that the DFT calculated interlayer coupling is on the order of $10^{-1}$ meV for $MnBi_4Te_7$ and $10^{-2}$ meV for $MnBi_6Te_{10}$, the reduced intralayer magnetization could play a more significant role in effectively reducing the interlayer coupling in $MnBi_6Te_{10}$ than $MnBi_4Te_7$. For pressurized $MnBi_4Te_7$, the experimentally increased $B_s$ and strongly suppressed hysteresis loops under high pressure indicate enhanced interlayer AFM coupling. However, for pressurized $MnBi_6Te_{10}$, $B_s$ decreases over pressure, and a quasi-2D FM state emerges after the weak AFM kinks disappear around 1.5 GPa, consistent with our scenario of reduced and eventually decoupled magnetic layers due to reduced intralayer FM coupling. Coincidentally, the saturation field of the pressure-induced FM phase in $MnBi_6Te_{10}$ is also comparable to what was observed in the FM axion insulator $MnBi_8Te_{13}$.[30,31] To confirm whether the lattice compression alters the topological nature of the band structure, we have performed theoretical calculations, and the details are listed in the Supporting Information (Figure S10 and Table S1). Under 0 and 2 GPa, both $MnBi_4Te_7$ and $MnBi_6Te_{10}$ exhibit robust topological nontrivial phases. Therefore, an FM topological state is expected in $MnBi_6Te_{10}$ when pressure tunes its magnetic phase to FM.

To further validate our understanding of the competing intralayer exchange coupling, we investigated the magnetic properties of Sb-doped $MnBi_6Te_{10}$, where the in-plane lattice constants are effectively reduced while the interlayer distance ($c$-axis lattice parameter) stays almost unchanged.[45−49] Compared with the pressurized case, since there is little lattice change along $c$-axis to enhance the interlayer coupling, the Sb-doped samples would enter the FM phase at a smaller intralayer lattice compression. We target 20% Sb-doped $MnBi_6Te_{10}$ sample, as the in-plane lattice constant change is near but slightly lower than that of the pressurized $MnBi_6Te_{10}$ near the phase transition from AFM to quasi-2D-FM state. The Sb-doped $MnBi_6Te_{10}$ crystals are prepared by replacing the Bi component with a molar ratio 1/4 of Sb to Bi in the original recipe. The actual composition is found to be $Mn_{0.77}Sb_{1.46}Bi_{4.54}Te_{9.54}$ by EDX, determined from the average of 18 randomly selected spots on three samples. The actual Sb concentration is about 1.2 times the nominal ratio, similar to Sb-doped $MnBi_4Te_7$.[48] Powder and single-crystal XRD results (Figure S11) show a 0.65% contraction of the in-plane lattice constant, while the out-of-plane lattice component stays around 101.985(8)Å (with a negligible increase of 0.07%). Interestingly, Figure 4a shows a large bifurcation of ZFC and FC curves at a magnetic ordering temperature of 11.3 K, which is similar to the FM behavior of $MnBi_8Te_{13}$[30,31] and pressurized $MnBi_6Te_{10}$ at 1.98 GPa (Figure 2a), but in contrast with the sharp cusp AFM feature of the parent compound.[27−29] Moreover, the magnetic susceptibility of Sb-doped $MnBi_6Te_{10}$ is one order larger than that of the parent. The magnetization curves with H//ab and H//c at different temperatures in Figure 4b also reveal a similar FM hysteresis loop as observed in the anomalous Hall effect of the parent at 1.98 GPa.

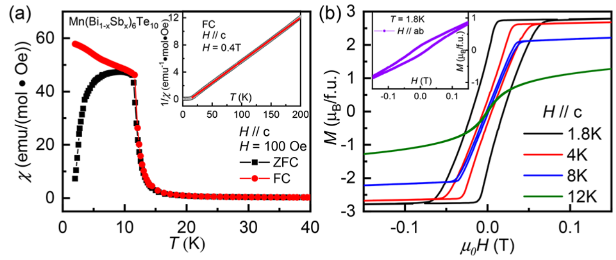


**Figure 4.** Temperature dependence of ZFC and FC magnetic susceptibility of Sb-doped $MnBi_6Te_{10}$ with an applied magnetic field of 100 Oe along the $c$-axis. The inset shows the temperature-dependent field cooled inverse susceptibility at $H$ = 0.4T for H//c, and the red line is the fitting result of Curie−Weiss law. (b) Isothermal magnetization curves of the Sb-doped $MnBi_6Te_{10}$ below 15 K for H//c and H//ab (the inset). The FM loops show no kinks or plateaus associated with AFM states up to the magnetic ordering temperature of 11.3 K.

The observation of such an FM state in Sb-doped $MnBi_6Te_{10}$ strongly supports our scenario that reduced intralayer FM coupling due to in-plane lattice compression can trigger the AFM to quasi-2D-FM phase transition in $MnBi_6Te_{10}$, similar to the pressurized case. It is worth noting that Sb doping may also promote $Mn^{Sb}$ antisite defects since the electronegativity and ionic size of Sb are closer to Mn than that of Bi. The exchange coupling between the original Mn and Mn occupied on Bi/Sb site within $MnBi_2Te_4$ layer is reported to be ferrimagnetic coupling,[46,48,50] which can also affect the magnetism. Considering the migration of Mn and other defects, the competition between intralayer and interlayer coupling can be more complicated, leading to complex magnetic phase transitions observed in $MnSb_2Te_4$ and heavily Sb-doped $MnBi_4Te_7$.[48−50] However, in our case, the Sb component is relatively small. The density of $Mn^{Sb/Bi}$ antisite defects is comparable to the parent (1% ∼ 2.1%) on the second atomic layer of the three terminations (Table S2), revealed by the scanning tunneling microscope images (Figure S13). We believe that the ferrimagnetic coupling induced by Sb doping does not play a dominant role in changing the magnetic properties. Unlike the coexistence of AFM and FM phases in Sb-doped $MnBi_4Te_7$ for a much higher doping level $x \sim 0.48$,[48] both the $M-T$ and $M-H$ curves of our 20% Sb-doped $MnBi_6Te_{10}$ show no signature of AFM phase. In addition, comparing with the reported ferrimagnetic behaviors in $MnSb_2Te_4$[46,47,50] and the heavily Sb-doped $MnBi_4Te_7$ (83%),[48] our 20% Sb-doped $MnBi_6Te_{10}$ shows a linear $1/\chi \sim T$ curve at paramagnetic state. The higher FC magnetic susceptibility (58 emu $mol^{-1}$ $Oe^{1-}$) and saturation moment at 2 K (2.84 $\mu_B$/Mn) are both close to those of the FM $MnBi_8Te_{13}$ (3.1 $\mu_B$/Mn).[30,31] Therefore, the successful realization of quasi-2D-FM state in Sb-doped $MnBi_6Te_{10}$ provides additional evidence that the intralayer coupling plays an important role in the magnetism of weakly coupled magnetic topological insulator heterostructures.

In summary, we have systematically studied the magnetic and magneto-transport properties of $MnBi_2Te_4(Bi_2Te_3)_n$ for $n$ = 1 and 2 under hydrostatic pressure up to 3.5 GPa. For $n$ = 1, the saturation field increases, and the Néel temperature decreases as increasing pressure due to an enhanced interlayer AFM coupling competing combined with a weakened intralayer FM coupling. For $n$ = 2, the interlayer AFM coupling is weak enough, so that as pressure increases, the


https://doi.org/10.1021/acs.nanolett.1c01874
Nano Lett. 2021, 21, 5874−5880

decreased intralayer FM exchange coupling can effectively reduce the interlayer exchange coupling, resulting in a magnetic phase transition from A-type AFM to a quasi-2D FM states at around 1.5 GPa. Our results show that the intralayer exchange coupling plays a significant role in determining the magnetic properties of weakly coupled $MnBi_2Te_4(Bi_2Te_3)_n$. The intralayer exchange coupling can be delicately tuned by lattice engineering, such as pressure and chemical substitution. We show that an intrinsic FM state can be realized in both pressurized $MnBi_6Te_{10}$ and Sb-doped $MnBi_6Te_{10}$. Our results shed light on the intriguing magnetism in the family of $MnBi_2Te_4(Bi_2Te_3)_n$ and open up opportunities for the realization of various topological phases determined by their magnetic phases.

## ■ METHODS

The single crystals were grown by flux method and confirmed by X-ray diffraction. Subsequent screening using magnetic and magneto-transport measurements were performed at physical property measurement system (PPMS). Hydrostatic pressure was applied by a self-clamped BeCu-NiCrAl double-wall piston−cylinder cell with a maximum pressure of 3.5 GPa, using Daphne 7373 oil as a pressure transmitting medium. The real Sb doping ratio was measured by energy-dispersive X-ray spectroscopy (EDX). The scanning tunneling microscope (STM) measurements were performed on *in situ* cleaved surfaces of $Mn(Bi_{1-x}Sb_x)_6Te_{10}$ using commercial STM (Unisoku USM 1300) operating at 77K.

## ■ ASSOCIATED CONTENT

### Supporting Information

The Supporting Information is available free of charge at https://pubs.acs.org/doi/10.1021/acs.nanolett.1c01874.

Single crystal growth method and structure characterization of $MnBi_4Te_7$ and $MnBi_6Te_{10}$; Magnetic and transport properties of the crystals at ambient pressure; Measurement details of the magneto-transport properties under high pressure; Magnetic susceptibility and magnetization of $MnBi_6Te_{10}$ under high pressure measured by precalibrated Hall sensor; DFT calculation method; Calculated lattice compression and topological properties under pressure for both $MnBi_4Te_7$ and $MnBi_6Te_{10}$; Crystal structure and magnetic properties of 20% Sb-doped $MnBi_6Te_{10}$; Defect statistics of $Mn(Bi_{1-x}Sb_x)_6Te_{10}$ ($x$ = 0 and 0.2) measured by scanning tunneling microscope (PDF)

## ■ AUTHOR INFORMATION

### Corresponding Authors

**Yue Zhao** − *Shenzhen Institute for Quantum Science and Engineering and Department of Physics, Southern University of Science and Technology, Shenzhen 518055, China;* orcid.org/0000-0002-9174-0519; Email: zhaoy@sustech.edu.cn

**Qihang Liu** − *Shenzhen Institute for Quantum Science and Engineering and Department of Physics, Guangdong Provincial Key Laboratory for Computational Science and Material Design, and Shenzhen Key Laboratory of for Advanced Quantum Functional Materials and Devices, Southern University of Science and Technology, Shenzhen 518055, China*; Email: liuqh@sustech.edu.cn

### Authors

**Jifeng Shao** − *Shenzhen Institute for Quantum Science and Engineering and Department of Physics, Southern University of Science and Technology, Shenzhen 518055, China;* orcid.org/0000-0001-6460-3423

**Yuntian Liu** − *Shenzhen Institute for Quantum Science and Engineering and Department of Physics, Southern University of Science and Technology, Shenzhen 518055, China*

**Meng Zeng** − *Shenzhen Institute for Quantum Science and Engineering and Department of Physics, Southern University of Science and Technology, Shenzhen 518055, China*

**Jingyuan Li** − *Shenzhen Institute for Quantum Science and Engineering and Department of Physics, Southern University of Science and Technology, Shenzhen 518055, China*

**Xuefeng Wu** − *Shenzhen Institute for Quantum Science and Engineering and Department of Physics, Southern University of Science and Technology, Shenzhen 518055, China*

**Xiao-Ming Ma** − *Shenzhen Institute for Quantum Science and Engineering and Department of Physics, Southern University of Science and Technology, Shenzhen 518055, China*

**Feng Jin** − *Hefei National Laboratory for Physical Sciences at Microscale, University of Science and Technology of China, Hefei 230026, China*

**Ruie Lu** − *Shenzhen Institute for Quantum Science and Engineering and Department of Physics, Southern University of Science and Technology, Shenzhen 518055, China*

**Yichen Sun** − *Shenzhen Institute for Quantum Science and Engineering and Department of Physics, Southern University of Science and Technology, Shenzhen 518055, China*

**Mingqiang Gu** − *Shenzhen Institute for Quantum Science and Engineering and Department of Physics, Southern University of Science and Technology, Shenzhen 518055, China*

**Kedong Wang** − *Shenzhen Institute for Quantum Science and Engineering and Department of Physics, Southern University of Science and Technology, Shenzhen 518055, China;* orcid.org/0000-0003-1253-5603

**Wenbin Wu** − *Hefei National Laboratory for Physical Sciences at Microscale, University of Science and Technology of China, Hefei 230026, China*

**Liusuo Wu** − *Shenzhen Institute for Quantum Science and Engineering and Department of Physics, Southern University of Science and Technology, Shenzhen 518055, China*

**Chang Liu** − *Shenzhen Institute for Quantum Science and Engineering and Department of Physics, Southern University of Science and Technology, Shenzhen 518055, China*

Complete contact information is available at: https://pubs.acs.org/10.1021/acs.nanolett.1c01874

### Author Contributions

[‖]J.S. and Y.L. contributed equally. Y.Z. and Q.L. are responsible for the project. M.Z., X.M. and R.L. performed the single crystal growth and XRD characterization. J.S. performed the whole magnetic and transport measurements at different pressures with J.L. and Y.S. F.J. and W.W. performed the magnetic measurement at ambient pressure. Y.L. performed the DFT calculations with the help from M.G. X.W. and K.W. performed the STM measurements. J.S., Y.L., C.L., Q.L., and Y.Z. analyzed the data. J.S., Y.L., Q.L., and Y.Z. wrote the paper, and all authors participated in the discussions of the results.

### Notes

The authors declare no competing financial interest.

## ■ ACKNOWLEDGMENTS

The research was supported by the Key-Area Research and Development Program of Guangdong Province (2019B010931001), National Natural Science Foundation of China under project Nos. 11674150, 11804402, U2032218, 11974326, 11804144, 11974157, 11804342, 12074161, National Key R&D Program of China (2019YFA0704900), Guangdong Innovative and Entrepreneurial Research Team Program (2016ZT06D348 and 2017ZT07C062), the Guangdong Provincial Key Laboratory of Computational Science and Material Design (Grant No. 2019B030301001), the Science, Technology, and Innovation Commission of Shenzhen Municipality (JCYJ20160613160524999, ZDSYS20190902092905285, G02206304 and G02206404), the Shenzhen Key Laboratory (Grant No. ZDSYS20170303165926217), the Highlight Project (No. PHYS-HL-2020-1) of the College of Science of SUSTech, and Hefei Science Center of Chinese Academy of Sciences (Grant 2018ZYFX002). First-principles calculations were also supported by Center for Computational Science and Engineering at SUSTech. We thank Junhao Lin for valuable discussions.

## ■ REFERENCES

(1) Qi, X.-L.; Hughes, T. L.; Zhang, S.-C. Topological field theory of time-reversal invariant insulators. *Phys. Rev. B: Condens. Matter Mater. Phys.* **2008**, *78* (19), 195424.

(2) Mong, R. S. K.; Essin, A. M.; Moore, J. E. Antiferromagnetic topological insulators. *Phys. Rev. B: Condens. Matter Mater. Phys.* **2010**, *81* (24), 245209.

(3) Wan, X. G.; Turner, A. M.; Vishwanath, A.; Savrasov, S. Y. Topological semimetal and Fermi-arc surface states in the electronic structure of pyrochlore iridates. *Phys. Rev. B: Condens. Matter Mater. Phys.* **2011**, *83* (20), 205101.

(4) Chang, C. Z.; Zhang, J.; Feng, X.; Shen, J.; Zhang, Z.; Guo, M.; Li, K.; Ou, Y.; Wei, P.; Wang, L. L.; Ji, Z. Q.; Feng, Y.; Ji, S.; Chen, X.; Jia, J.; Dai, X.; Fang, Z.; Zhang, S. C.; He, K.; Wang, Y.; Lu, L.; Ma, X. C.; Xue, Q. K. Experimental observation of the quantum anomalous Hall effect in a magnetic topological insulator. *Science* **2013**, *340* (6129), 167−170.

(5) Wang, D.; Kong, L.; Fan, P.; Chen, H.; Zhu, S.; Liu, W.; Cao, L.; Sun, Y.; Du, S.; Schneeloch, J.; Zhong, R.; Gu, G.; Fu, L.; Ding, H.; Gao, H. J. Evidence for Majorana bound states in an iron-based superconductor. *Science* **2018**, *362* (6412), 333−335.

(6) Tokura, Y.; Yasuda, K.; Tsukazaki, A. Magnetic topological insulators. *Nat. Rev. Phys.* **2019**, *1* (2), 126−143.

(7) Cui, J.; Shi, M.; Wang, H.; Yu, F.; Wu, T.; Luo, X.; Ying, J.; Chen, X. Transport properties of thin flakes of the antiferromagnetic topological insulator $MnBi_2Te_4$. *Phys. Rev. B: Condens. Matter Mater. Phys.* **2019**, *99* (15), 155125.

(8) Gong, Y.; Guo, J.; Li, J.; Zhu, K.; Liao, M.; Liu, X.; Zhang, Q.; Gu, L.; Tang, L.; Feng, X.; Zhang, D.; Li, W.; Song, C.; Wang, L.; Yu, P.; Chen, X.; Wang, Y.; Yao, H.; Duan, W.; Xu, Y.; Zhang, S.-C.; Ma, X.; Xue, Q.-K.; He, K. Experimental Realization of an Intrinsic Magnetic Topological Insulator. *Chin. Phys. Lett.* **2019**, *36* (7), 076801.

(9) Hao, Y.-J.; Liu, P.; Feng, Y.; Ma, X.-M.; Schwier, E. F.; Arita, M.; Kumar, S.; Hu, C.; Lu, R. e.; Zeng, M.; Wang, Y.; Hao, Z.; Sun, H.-Y.; Zhang, K.; Mei, J.; Ni, N.; Wu, L.; Shimada, K.; Chen, C.; Liu, Q.; Liu, C. Gapless Surface Dirac Cone in Antiferromagnetic Topological Insulator $MnBi_2Te_4$. *Phys. Rev. X* **2019**, *9* (4), 041038.

(10) Lee, S. H.; Zhu, Y.; Wang, Y.; Miao, L.; Pillsbury, T.; Yi, H.; Kempinger, S.; Hu, J.; Heikes, C. A.; Quarterman, P.; Ratcliff, W.; Borchers, J. A.; Zhang, H.; Ke, X.; Graf, D.; Alem, N.; Chang, C.-Z.; Samarth, N.; Mao, Z. Spin scattering and noncollinear spin structure-induced intrinsic anomalous Hall effect in antiferromagnetic topological insulator $MnBi_2Te_4$. *Phys. Rev. Research* **2019**, *1* (1), 012011.

(11) Otrokov, M. M.; Klimovskikh, I. I.; Bentmann, H.; Estyunin, D.; Zeugner, A.; Aliev, Z. S.; Gass, S.; Wolter, A. U. B.; Koroleva, A. V.; Shikin, A. M.; Blanco-Rey, M.; Hoffmann, M.; Rusinov, I. P.; Vyazovskaya, A. Y.; Eremeev, S. V.; Koroteev, Y. M.; Kuznetsov, V. M.; Freyse, F.; Sanchez-Barriga, J.; Amiraslanov, I. R.; Babanly, M. B.; Mamedov, N. T.; Abdullayev, N. A.; Zverev, V. N.; Alfonsov, A.; Kataev, V.; Buchner, B.; Schwier, E. F.; Kumar, S.; Kimura, A.; Petaccia, L.; Di Santo, G.; Vidal, R. C.; Schatz, S.; Kissner, K.; Unzelmann, M.; Min, C. H.; Moser, S.; Peixoto, T. R. F.; Reinert, F.; Ernst, A.; Echenique, P. M.; Isaeva, A.; Chulkov, E. V. Prediction and observation of an antiferromagnetic topological insulator. *Nature* **2019**, *576* (7787), 416−422.

(12) Sass, P. M.; Ge, W.; Yan, J.; Obeysekera, D.; Yang, J. J.; Wu, W. Magnetic Imaging of Domain Walls in the Antiferromagnetic Topological Insulator $MnBi_2Te_4$. *Nano Lett.* **2020**, *20* (4), 2609−2614.

(13) Li, J.; Li, Y.; Du, S.; Wang, Z.; Gu, B. L.; Zhang, S. C.; He, K.; Duan, W.; Xu, Y. Intrinsic magnetic topological insulators in van der Waals layered $MnBi_2Te_4$-family materials. *Sci. Adv.* **2019**, *5* (6), eaaw5685.

(14) Otrokov, M. M.; Rusinov, I. P.; Blanco-Rey, M.; Hoffmann, M.; Vyazovskaya, A. Y.; Eremeev, S. V.; Ernst, A.; Echenique, P. M.; Arnau, A.; Chulkov, E. V. Unique Thickness-Dependent Properties of the van der Waals Interlayer Antiferromagnet $MnBi_2Te_4$ films. *Phys. Rev. Lett.* **2019**, *122* (10), 107202.

(15) Zhang, D.; Shi, M.; Zhu, T.; Xing, D.; Zhang, H.; Wang, J. Topological Axion States in the Magnetic Insulator $MnBi_2Te_4$ with the Quantized Magnetoelectric Effect. *Phys. Rev. Lett.* **2019**, *122* (20), 206401.

(16) Deng, Y.; Yu, Y.; Shi, M. Z.; Guo, Z.; Xu, Z.; Wang, J.; Chen, X. H.; Zhang, Y. Quantum anomalous Hall effect in intrinsic magnetic topological insulator $MnBi_2Te_4$. *Science* **2020**, *367* (6480), 895−900.

(17) Ge, J.; Liu, Y.; Li, J.; Li, H.; Luo, T.; Wu, Y.; Xu, Y.; Wang, J. High-Chern-number and high-temperature quantum Hall effect without Landau levels. *Natl. Sci. Rev.* **2020**, *7* (8), 1280−1287.

(18) Liu, C.; Wang, Y.; Li, H.; Wu, Y.; Li, Y.; Li, J.; He, K.; Xu, Y.; Zhang, J.; Wang, Y. Robust axion insulator and Chern insulator phases in a two-dimensional antiferromagnetic topological insulator. *Nat. Mater.* **2020**, *19* (5), 522−527.

(19) Sun, H.; Xia, B.; Chen, Z.; Zhang, Y.; Liu, P.; Yao, Q.; Tang, H.; Zhao, Y.; Xu, H.; Liu, Q. Rational Design Principles of the Quantum Anomalous Hall Effect in Superlatticelike Magnetic Topological Insulators. *Phys. Rev. Lett.* **2019**, *123* (9), 096401.

(20) Aliev, Z. S.; Amiraslanov, I. R.; Nasonova, D. I.; Shevelkov, A. V.; Abdullayev, N. A.; Jahangirli, Z. A.; Orujlu, E. N.; Otrokov, M. M.; Mamedov, N. T.; Babanly, M. B.; Chulkov, E. V. Novel ternary layered manganese bismuth tellurides of the MnTe-$Bi_2Te_3$ system: Synthesis and crystal structure. *J. Alloys Compd.* **2019**, *789*, 443−450.

(21) Vidal, R. C.; Zeugner, A.; Facio, J. I.; Ray, R.; Haghighi, M. H.; Wolter, A. U. B.; Bohorquez, L. T. C.; Caglieris, F.; Moser, S.; Figgemeier, T.; Peixoto, T. R. F.; Vasili, H. B.; Valvidares, M.; Jung, S.; Cacho, C.; Alfonsov, A.; Mehlawat, K.; Kataev, V.; Hess, C.; Richter, M.; Buchner, B.; van den Brink, J.; Ruck, M.; Reinert, F.; Bentmann, H.; Isaeva, A. Topological Electronic Structure and Intrinsic Magnetization in $MnBi_4Te_7$: A $Bi_2Te_3$ Derivative with a Periodic Mn Sublattice. *Phys. Rev. X* **2019**, *9* (4), 041065.

(22) Wu, J.; Liu, F.; Sasase, M.; Ienaga, K.; Obata, Y.; Yukawa, R.; Horiba, K.; Kumigashira, H.; Okuma, S.; Inoshita, T.; Hosono, H. Natural van der Waals heterostructural single crystals with both magnetic and topological properties. *Sci. Adv.* **2019**, *5* (11), eaax9989.

(23) Ding, L.; Hu, C.; Ye, F.; Feng, E.; Ni, N.; Cao, H. Crystal and magnetic structures of magnetic topological insulators $MnBi_2Te_4$ and $MnBi_4Te_7$. *Phys. Rev. B: Condens. Matter Mater. Phys.* **2020**, *101* (2), 020412.

(24) Hu, C.; Gordon, K. N.; Liu, P.; Liu, J.; Zhou, X.; Hao, P.; Narayan, D.; Emmanouilidou, E.; Sun, H.; Liu, Y.; Brawer, H.; Ramirez, A. P.; Ding, L.; Cao, H.; Liu, Q.; Dessau, D.; Ni, N. A van

der Waals antiferromagnetic topological insulator with weak interlayer magnetic coupling. *Nat. Commun.* **2020**, *11* (1), 97.

(25) Wu, X.; Li, J.; Ma, X.-M.; Zhang, Y.; Liu, Y.; Zhou, C.-S.; Shao, J.; Wang, Q.; Hao, Y.-J.; Feng, Y.; Schwier, E. F.; Kumar, S.; Sun, H.; Liu, P.; Shimada, K.; Miyamoto, K.; Okuda, T.; Wang, K.; Xie, M.; Chen, C.; Liu, Q.; Liu, C.; Zhao, Y. Distinct Topological Surface States on the Two Terminations of $MnBi_4Te_7$. *Phys. Rev. X* **2020**, *10* (3), 031013.

(26) Yan, J. Q.; Liu, Y. H.; Parker, D. S.; Wu, Y.; Aczel, A. A.; Matsuda, M.; McGuire, M. A.; Sales, B. C. A-type antiferromagnetic order in $MnBi_4Te_7$ and $MnBi_6Te_{10}$ single crystals. *Phys. Rev. Mater.* **2020**, *4* (5), 054202.

(27) Shi, M. Z.; Lei, B.; Zhu, C. S.; Ma, D. H.; Cui, J. H.; Sun, Z. L.; Ying, J. J.; Chen, X. H. Magnetic and transport properties in the magnetic topological insulators $MnBi_2Te_4(Bi_2Te_3)_n$ (n = 1,2). *Phys. Rev. B: Condens. Matter Mater. Phys.* **2019**, *100* (15), 155144.

(28) Ma, X.-M.; Chen, Z.; Schwier, E. F.; Zhang, Y.; Hao, Y.-J.; Kumar, S.; Lu, R.; Shao, J.; Jin, Y.; Zeng, M.; Liu, X.-R.; Hao, Z.; Zhang, K.; Mansuer, W.; Song, C.; Wang, Y.; Zhao, B.; Liu, C.; Deng, K.; Mei, J.; Shimada, K.; Zhao, Y.; Zhou, X.; Shen, B.; Huang, W.; Liu, C.; Xu, H.; Chen, C. Hybridization-induced gapped and gapless states on the surface of magnetic topological insulators. *Phys. Rev. B: Condens. Matter Mater. Phys.* **2020**, *102* (24), 245136.

(29) Tian, S.; Gao, S.; Nie, S.; Qian, Y.; Gong, C.; Fu, Y.; Li, H.; Fan, W.; Zhang, P.; Kondo, T.; Shin, S.; Adell, J.; Fedderwitz, H.; Ding, H.; Wang, Z.; Qian, T.; Lei, H. Magnetic topological insulator $MnBi_6Te_{10}$ with a zero-field ferromagnetic state and gapped Dirac surface states. *Phys. Rev. B: Condens. Matter Mater. Phys.* **2020**, *102* (3), 035144.

(30) Hu, C.; Ding, L.; Gordon, K. N.; Ghosh, B.; Tien, H. J.; Li, H.; Linn, A. G.; Lien, S. W.; Huang, C. Y.; Mackey, S.; Liu, J.; Reddy, P. V. S.; Singh, B.; Agarwal, A.; Bansil, A.; Song, M.; Li, D.; Xu, S. Y.; Lin, H.; Cao, H.; Chang, T. R.; Dessau, D.; Ni, N. Realization of an intrinsic ferromagnetic topological state in $MnBi_8Te_{13}$. *Sci. Adv.* **2020**, *6* (30), eaba4275.

(31) Lu, R.; Sun, H.; Kumar, S.; Wang, Y.; Gu, M.; Zeng, M.; Hao, Y.-J.; Li, J.; Shao, J.; Ma, X.-M.; Hao, Z.; Zhang, K.; Mansuer, W.; Mei, J.; Zhao, Y.; Liu, C.; Deng, K.; Huang, W.; Shen, B.; Shimada, K.; Schwier, E. F.; Liu, C.; Liu, Q.; Chen, C. Half-Magnetic Topological Insulator with Magnetization-Induced Dirac Gap at a Selected Surface. *Phys. Rev. X* **2021**, *11* (1), 011039.

(32) Tan, A.; Labracherie, V.; Kunchur, N.; Wolter, A. U. B.; Cornejo, J.; Dufouleur, J.; Buchner, B.; Isaeva, A.; Giraud, R. Metamagnetism of Weakly Coupled Antiferromagnetic Topological Insulators. *Phys. Rev. Lett.* **2020**, *124* (19), 197201.

(33) Li, T.; Jiang, S.; Sivadas, N.; Wang, Z.; Xu, Y.; Weber, D.; Goldberger, J. E.; Watanabe, K.; Taniguchi, T.; Fennie, C. J.; Fai Mak, K.; Shan, J. Pressure-controlled interlayer magnetism in atomically thin $CrI_3$. *Nat. Mater.* **2019**, *18* (12), 1303−1308.

(34) Song, T.; Fei, Z.; Yankowitz, M.; Lin, Z.; Jiang, Q.; Hwangbo, K.; Zhang, Q.; Sun, B.; Taniguchi, T.; Watanabe, K.; McGuire, M. A.; Graf, D.; Cao, T.; Chu, J. H.; Cobden, D. H.; Dean, C. R.; Xiao, D.; Xu, X. Switching 2D magnetic states via pressure tuning of layer stacking. *Nat. Mater.* **2019**, *18* (12), 1298−1302.

(35) Yankowitz, M.; Chen, S.; Polshyn, H.; Zhang, Y.; Watanabe, K.; Taniguchi, T.; Graf, D.; Young, A. F.; Dean, C. R. Tuning superconductivity in twisted bilayer graphene. *Science* **2019**, *363* (6431), 1059−1064.

(36) Fülöp, B.; Márffy, A.; Zihlmann, S.; Gmitra, M.; Tóvári, E.; Szentpéteri, B.; Kedves, M.; Watanabe, K.; Taniguchi, T.; Fabian, J.; Schönenberger, C.; Makk, P.; Csonka, S. Boosting proximity spin orbit coupling in graphene/$WSe_2$ heterostructures via hydrostatic pressure. **2021**, arXiv:2103.13325v1. *arXiv.org e-Print archive.* https://arxiv.org/abs/2103.13325 (accessed on March 24, 2021).

(37) Zhang, J. L.; Zhang, S. J.; Weng, H. M.; Zhang, W.; Yang, L. X.; Liu, Q. Q.; Feng, S. M.; Wang, X. C.; Yu, R. C.; Cao, L. Z.; Wang, L.; Yang, W. G.; Liu, H. Z.; Zhao, W. Y.; Zhang, S. C.; Dai, X.; Fang, Z.; Jin, C. Q. Pressure-induced superconductivity in topological parent compound $Bi_2Te_3$. *Proc. Natl. Acad. Sci. U. S. A.* **2011**, *108* (1), 24−28.

(38) Chen, K. Y.; Wang, B. S.; Yan, J. Q.; Parker, D. S.; Zhou, J. S.; Uwatoko, Y.; Cheng, J. G. Suppression of the antiferromagnetic metallic state in the pressurized $MnBi_2Te_4$ single crystal. *Phys. Rev. Mater.* **2019**, *3* (9), 094201.

(39) Pei, C.; Xia, Y.; Wu, J.; Zhao, Y.; Gao, L.; Ying, T.; Gao, B.; Li, N.; Yang, W.; Zhang, D.; Gou, H.; Chen, Y.; Hosono, H.; Li, G.; Qi, Y. Pressure-Induced Topological and Structural Phase Transitions in an Antiferromagnetic Topological Insulator. *Chin. Phys. Lett.* **2020**, *37* (6), 066401.

(40) Goodenough, J. B. Theory of the Role of Covalence in the Perovskite-Type Manganites [La, M(II)]$MnO_3$. *Phys. Rev.* **1955**, *100* (2), 564−573.

(41) Anderson, P. W. New Approach to the Theory of Superexchange Interactions. *Phys. Rev.* **1959**, *115* (1), 2−13.

(42) Mehl, M. J.; Papaconstantopoulos, D. A. Applications of a tight-binding total-energy method for transition and noble metals: Elastic constants, vacancies, and surfaces of monatomic metals. *Phys. Rev. B: Condens. Matter Mater. Phys.* **1996**, *54* (7), 4519−4530.

(43) Li, X.; Yang, J. $CrXTe_3$(X = Si, Ge) nanosheets: two dimensional intrinsic ferromagnetic semiconductors. *J. Mater. Chem. C* **2014**, *2* (34), 7071−7076.

(44) Chen, B.; Xu, H.; Ma, C.; Mattauch, S.; Lan, D.; Jin, F.; Guo, Z.; Wan, S.; Chen, P.; Gao, G.; Chen, F.; Su, Y.; Wu, W. All-oxide-based synthetic antiferromagnets exhibiting layer-resolved magnetization reversal. *Science* **2017**, *357* (6347), 191−194.

(45) Chen, B.; Fei, F.; Zhang, D.; Zhang, B.; Liu, W.; Zhang, S.; Wang, P.; Wei, B.; Zhang, Y.; Zuo, Z.; Guo, J.; Liu, Q.; Wang, Z.; Wu, X.; Zong, J.; Xie, X.; Chen, W.; Sun, Z.; Wang, S.; Zhang, Y.; Zhang, M.; Wang, X.; Song, F.; Zhang, H.; Shen, D.; Wang, B. Intrinsic magnetic topological insulator phases in the Sb doped $MnBi_2Te_4$ bulks and thin flakes. *Nat. Commun.* **2019**, *10* (1), 4469.

(46) Murakami, T.; Nambu, Y.; Koretsune, T.; Xiangyu, G.; Yamamoto, T.; Brown, C. M.; Kageyama, H. Realization of interlayer ferromagnetic interaction in $MnSb_2Te_4$ toward the magnetic Weyl semimetal state. *Phys. Rev. B: Condens. Matter Mater. Phys.* **2019**, *100* (19), 195103.

(47) Yan, J. Q.; Okamoto, S.; McGuire, M. A.; May, A. F.; McQueeney, R. J.; Sales, B. C. Evolution of structural, magnetic, and transport properties in $MnBi_{2-x}Sb_xTe_4$. *Phys. Rev. B: Condens. Matter Mater. Phys.* **2019**, *100* (10), 104409.

(48) Hu, C.; Mackey, S.; Ni, N. Switching on ferromagnetic coupling by Mn/Sb antisite disorder in $Mn(Bi_{1-x}Sb_x)_4Te_7$:from electron-doped antiferromagnet to hole-doped ferrimagnet. **2020**, arXiv:2008.09097v1. *arXiv.org e-Print archive.* https://arxiv.org/abs/2008.09097v1 (accessed on August 20, 2020).

(49) Chen, B.; Fei, F.; Wang, D.; Jiang, Z.; Zhang, B.; Guo, J.; Xie, H.; Zhang, Y.; Naveed, M.; Du, Y.; Sun, Z.; Zhang, H.; Shen, D.; Song, F. Coexistence of Ferromagnetism and Topology by Charge Carrier Engineering in intrinsic magnetic topological insulator $MnBi_4Te_7$. **2020**, arXiv:2009.00039v1. *arXiv.org e-Print archive.* https://arxiv.org/abs/2009.00039v1 (accessed on August 31, 2020).

(50) Liu, Y.; Wang, L.-L.; Zheng, Q.; Huang, Z.; Wang, X.; Chi, M.; Wu, Y.; Chakoumakos, B. C.; McGuire, M. A.; Sales, B. C.; Wu, W.; Yan, J. Site Mixing for Engineering Magnetic Topological Insulators. *Phys. Rev. X* **2021**, *11* (2), 021033.



https://doi.org/10.1021/acs.nanolett.1c01874
*Nano Lett.* 2021, 21, 5874−5880